Bloch oscillations of topological edge modes

Chunyan Li,[1,2] Weifeng Zhang,[2] Yaroslav V. Kartashov,[3,4] Dmitry V. Skryabin,[5] and Fangwei Ye[2,6,*]

[1]*School of Physics and Optoelectronic Engineering, Xidian University, Xi'an 710071, China*

[2]*Key Laboratory for Laser Plasma (Ministry of Education), Collaborative Innovation Center of IFSA, School of Physics and Astronomy, Shanghai Jiao Tong University, Shanghai 200240, China*

[3]*ICFO-Institut de Ciencies Fotoniques, The Barcelona Institute of Science and Technology, 08860, Castelldefels (Barcelona), Spain*

[4]*Institute of Spectroscopy, Russian Academy of Sciences, Troitsk, Moscow, 108840, Russia*

[5]*Department of Physics, University of Bath, BA2 7AY Bath, United Kingdom*

[6]*Department of Physics, Zhejiang Normal University, Jinhua 321004, China*

(Received 22 September 2018; published 9 May 2019)

Under the action of a weak constant force a wave packet in periodic potential undergoes periodic oscillations in space, returning to the initial position after one oscillation cycle. This wave phenomenon, known as Bloch oscillations (BOs), pertains to many physical systems. Can BOs also occur in topological insulators with topologically protected edge states? This question is highly nontrivial, because in topological insulators with broken time-reversal symmetry, the edge states propagate unidirectionally without backscattering, hence BOs that typically involve stages, where a wave packet moves along and against the direction of the force, seem to be impossible in such systems when force acts parallel to the edge of the insulator. Here we reveal that BOs still occur with topological edge states, but in a nonconventional way: they are accompanied not only by oscillations along the edge in the direction of force, but also by oscillations in the direction transverse to that of the force. A full BO cycle involves switching between edge states at the opposite edges through delocalized bulk modes. Bloch oscillations of the topological edge states require to scan the first Brillouin zone twice to complete one cycle, thus they have a period that is two times larger than the period of usual BOs. All these unusual properties are in contrast to BOs in nontopological systems.

DOI: 10.1103/PhysRevA.99.053814

I. INTRODUCTION

Bloch oscillations (BOs) were introduced in seminal works that addressed the electron dynamics in crystalline lattices under the action of a constant electric field [1,2]. They were observed for electrons in semiconductor superlattices [3,4], shortly after the observation of Wannier-Stark ladders [5,6]. As a universal wave phenomenon, BOs have been shown to occur in a variety of physical systems, including ultracold atoms [7,8], Bose-Einstein condensates trapped in optical lattices [9–11], waveguide arrays [12–17], optically induced lattices [18,19], surface plasmon waves in plasmonic waveguides [20], and parity-time symmetric systems [21].

In contrast to conventional insulators, topological insulators [22,23] conduct at the edges of the structure and insulate in the bulk. The edge conductance is due to the existence of in-gap states that are spatially localized at the boundaries, propagate unidirectionally, and are immune to scattering by perturbations or disorder. Such a robustness is a consequence of topological protection [22,23]. The first observations of topological insulator states were performed in electronic systems and recently studies have been extended to electromagnetic waves [24]. Topological edge states have been proposed and observed in gyromagnetic photonic crystals [25,26], semiconductor quantum wells [27], arrays of coupled resonators [28,29], metamaterial superlattices [30], helical waveguide arrays [31,32], and in polariton microcavities, where strong photon-exciton coupling leads to the formation of half-light half-matter polariton quasiparticles [33–39], see [40] for recent experimental realization of a polariton topological insulator. Remarkably, application of a constant force to unbounded topological systems has been shown to provide a powerful tool for the measurement of its topological invariants [41–44]. It should be stressed that none of these works addressed Bloch oscillations in truncated topological insulators.

Here we combine the physics of topological insulators with BOs and introduce unusual BOs of topological edge states. Taking into account their unidirectional propagation nature at the edges, topological edge states at first glance cannot undergo BOs, because the latter implies that the wave packet periodically returns to its initial position. Our study reveals that the BOs of topological edge states are still possible, but in a form that sharply contrasts with BOs in the nontopological systems: although they are not able to propagate back and forth along the same side to complete BOs, topologial edge states still manage to restore their initial position periodically by switching into their counterpart at the other side of the structure that is propagating in the opposite direction. Thus, the BOs of a topological edge state involves not only longitudinal oscillations along the gradient, but also involves oscillations between the two edges of the topological insulator, which do not occur in nontopological systems. Furthermore, in corresponding momentum space the wave packet evolution

*fangweiye@sjtu.edu.cn

in the course of BOs connects the energy bands surrounding the topological gap and therefore induce nearly complete interband transitions even for very small gradients. This is in contrast to the usual Landau-Zener tunneling that occurs in nontopological systems, which remains noncomplete even for large gradients [45].

In this work we address BOs emerging in *truncated* topological insulators based on the microcavity exciton-polaritons model, however, the results can be carried over to a variety of other topological systems. BOs in topological systems may be investigated also in helical waveguide arrays with topological gap [46], especially if radiative losses can be reduced to an extent that a complete oscillation cycle can be observed. Also, some mathematical aspects of topological Bloch oscillations on infinite lattices, not involving edge states, are discussed in [47].

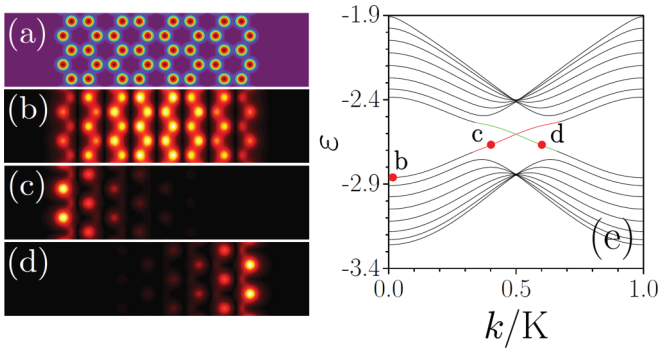

FIG. 1. (a) Schematic illustration showing lattice of microcavity pillars with zigzag-zigzag edges and (b)–(d) examples of modulus distributions of dominating component $|\psi_-|$ in modes, corresponding to the points **b–d** on the energy-momentum diagram (e). In all cases $\beta = 0.3$ and $\Omega = +0.8$.

II. MODEL

To provide an example of a topological system, where BOs are possible, we consider an exciton-polariton topological insulator based on microcavity whose top mirror is structured into a honeycomb lattice truncated on two sides. The resulting structure is a honeycomb lattice ribbon with zigzag edges in one direction and infinite along the other direction. The linear potential inducing Bloch oscillations features a gradient parallel to the ribbon edges. For the experimental realization of such a gradient in a polaritonic microcavity see, e.g., Ref. [48].

We address the evolution of a spinor polariton wave function $\boldsymbol{\psi} = (\psi_+, \psi_-)^{\mathrm{T}}$ governed by the coupled Schrödinger equations [33,39]:

$$i\frac{\partial \boldsymbol{\psi}}{\partial t} = -\frac{1}{2}\left(\partial_x^2 + \partial_y^2\right)\boldsymbol{\psi} + \sigma_1\beta(\partial_x \mp i\partial_y)^2\boldsymbol{\psi} + \sigma_3\Omega\boldsymbol{\psi} + [\mathcal{R}(x,y) + \alpha y]\boldsymbol{\psi}, \quad (1)$$

where x, y are the coordinates scaled to the characteristic length x_0; all energy parameters (such as the potential depth and the Zeeman splitting) are scaled to $\varepsilon_0 = \hbar^2/mx_0^2$, where m is the effective polariton mass that corresponds to the gradient and periodic potential free system; t is the evolution time scaled to $t_0 = \hbar\varepsilon_0^{-1}$; ψ_+ and ψ_- are the spin-positive and spin-negative components of the wave function in the circular polarization basis [33]; σ_1, σ_3 are the Pauli matrices; β is the strength of spin-orbit coupling arising from the fact that tunneling between microcavity pillars is polarization dependent; Ω is the Zeeman splitting; the potential landscape $\mathcal{R}(x,y) = -p\sum_{m,n}\mathcal{Q}(x - x_m, y - y_n)$ created by microcavity pillars arranged into a honeycomb array with nodes at the points (x_m, y_n) is composed of Gaussian wells $\mathcal{Q}(x,y) = \exp[-(x^2+y^2)/d^2]$ of characteristic diameter $2d$, depth p, and separation a between neighboring wells; the parameter $\alpha = Fx_0/\varepsilon_0$ describes a small dimensionless gradient along y that is necessary for the occurrence of BOs. We assume that the array of microcavity pillars is periodic along the y axis with a period $Y = 3^{1/2}a$ and that it is truncated along the x axis in such a way that the topological insulator acquires two zigzag edges [see two y periods of this structure in Fig. 1(a)]. A potential gradient is applied along the edges of the insulator. For $x_0 = 2$ μm and effective mass $m = 10^{-34}$ kg, one gets $\varepsilon_0 \approx 0.17$ meV and $t_0 \approx 3.8$ ps. We set $p = 8$, which corresponds to 1.38 meV, $d = 0.4$ (1.6 μm diameter), and $a = 1.4$ (2.8 μm separation between pillars). A potential energy gradient in the microcavity can be created by slight variations of its thickness along the y axis, as realized experimentally in [48]. Here we consider dimensionless gradients in the range $\alpha = 0.001$–0.01 (i.e., $F = 0.085$–0.85 meV/mm for characteristic parameters mentioned above). Note that such potential gradients are from two to one orders of magnitude smaller than gradients $\sim$10.5 meV/mm experimentally reported in [48]. For the largest gradient considered here the maximal displacement $\sim$35 μm of the wave packet upon evolution (see Fig. 4) leads to gradient-mediated polariton energy variation of $\sim$0.06 meV, as opposed to energy variations $\sim$20 meV observed experimentally. Still even for such energy gradients the effective mass was changing in [48] by less than 10%, which allows us to consider an effective mass (and also interactions) constant across the sample. This also means that the standard assumption about smallness of variation of the potential on one period due to gradient is valid, so that the influence of the gradient on the profiles of Bloch modes is negligible. The main effect of this potential is to trigger the variation of Bloch momentum of the wave packet in the Brillouin zone, as discussed below. Since the very fact of existence of the edge states in a topological polariton insulator is not connected with the presence of losses that are intrinsic in these systems and since Bloch oscillations are essentially linear physical phenomenon, we do not take losses into account in the model (1) and mention that such losses can be in principle compensated by the external pump, see, e.g., [49–52]. Moreover, recent progress in the technology of fabrication of high-Q microcavities with low losses [53,54] enabled a demonstration of long-living polariton condensates with lifetimes of several hundred picoseconds. It should be also mentioned that in the experiment, the pump (either coherent or incoherent) can be switched off after the relatively low polariton and reservoir exciton densities are created (i.e., after the initial state is prepared) so that any additional pump-induced energy shifts can be disregarded. Spatial distributions in subsequent dissipative dynamics will not be affected by losses, except for an overall decrease of density with time.

III. RESULTS AND DISCUSSION

The dynamics of Bloch oscillations is known to be strongly affected by the specific features of the Floquet-Bloch spectrum of the eigenmodes of the periodic structure at $\alpha = 0$. Here we aim to elucidate the new phenomena introduced by the unusual spectrum of the topological system. We first set $\alpha = 0$ in Eq. (1) and search for Bloch eigenmodes of the polariton topological insulator in the form $\boldsymbol{\psi}(x, y) = e^{iky - i\varepsilon(k)t}\boldsymbol{\phi}(x, y)$, where $\varepsilon(k)$ is the energy, $k \in [0, K]$ is the Bloch momentum along the y axis, $K = 2\pi/Y$ is the width of the Brillouin zone, and $\boldsymbol{\phi}(x, y) = \boldsymbol{\phi}(x, y + Y)$ is the periodic spinor function localized along the x axis. The lowest part of the spectrum of our structure is shown in Fig. 1(e), for the case when simultaneous action of spin-orbit coupling (here we took $\beta = 0.3$) and Zeeman splitting $\Omega = 0.8$ results in the breakup of time-reversal symmetry in Eq. (1) and opening of the topological gap between the first and second spectral bands, which in the absence of the above mentioned physical effects would meet at two Dirac points at $k = K/3$ and $k = 2K/3$. We deliberately selected a sufficiently large value of the Zeeman splitting to ensure a considerable separation in energy between the two depicted bands and the rest of the spectrum. This allows us to considerably suppress Landau-Zener tunneling into higher bands. Due to the truncation of the topological insulator, two unidirectional in-gap edge states connecting two bands arise at $K/3 < k < 2K/3$ [green and red curves in Fig. 1(e)]. Edge states belonging to different branches are highly confined near the zigzag edges, when their energies ε fall close to the center of the topological gap. See examples in Figs. 1(c) and 1(d) corresponding to the points **c** and **d** in Fig. 1(e). However, they notably expand into the bulk of the array when the energy approaches the edge of the topological gap. For $k \to 0$ or $k \to K$ such modes smoothly transform into bulk states. Thus, the bulk state from Fig. 1(b) resides in the same continuous branch of the dispersion relation (point **b**) as the edge state from Fig. 1(c) (point **c**).

In the presence of a potential gradient in Eq. (1) the wave packet experiences a constant force along y. If the force is small ($\alpha \ll 1$), the evolution of the system is adiabatic: one can operate with the same set of eigenmodes, but under the action of the force the Bloch momentum of the wave in our narrow lattice ribbon slowly varies in time, $k(t) = k_0 + \alpha t$, scanning the whole Brillouin zone [1]. Therefore, the Bloch wave with a broad envelope and momentum k_0 moves along the corresponding branch of the dispersion relation, undergoing shape transformations in real space that reflect the modification of the wave packet position in the spectrum from Fig. 1(e). Since the dependence $\varepsilon(k)$ is periodic, the evolution in the spatial domain is periodic too, if the Landau-Zener tunneling to higher bands is weak [2], which is the case in our system. If one uses for construction of a broad wave packet one of the modes from the depth of the first or second bands in Fig. 1(e), the wave packet moves along the corresponding branch of the dispersion relation, remaining always in the bulk of the array, undergoing conventional BOs with period $T = K/\alpha$. The same standard dynamics of BOs (without any interband transitions and switching between different edges) is observed in the nontopological system, where either spin-orbit coupling is set to zero ($\beta = 0$) or Zeeman splitting is absent ($\Omega = 0$) (recall that in such a system edge states are degenerate and there is no topological gap, hence a wave packet exciting mode from a certain branch always remains in the same band).

The picture changes qualitatively when the wave packet is constructed using topologically protected edge states at $\beta, \Omega \neq 0$ with broad y envelope (of width $w = 30$), such as the state with Bloch momentum $k_0 = 0.4$ K corresponding to the point **c** in Fig. 1(e). Examples of the evolution dynamics are presented in Fig. 2. The selected edge state has positive group velocity $v(k) = d\varepsilon/dk$, and it moves in the positive direction of the y axis. The state connects two different bands. Therefore, upon motion along the excited branch of the dispersion relation under the action of the constant force, the wave packet traverses the topological gap and for $\alpha > 0$ it transforms into a bulk state from the bottom of the second band. In real space this is accompanied by a considerable displacement along the y axis and by a shift of the wave packet into the bulk [see Fig. 2(b) at one quarter of the BO period]. Moving along the dispersion branch on the bottom of the second band, the wave packet reaches the point $k = K$ and due to the periodicity of dispersion, reappears at $k = 0$. In this point the group velocity changes its sign. Further variation of Bloch momentum induced by the force shifts the wave packet back into the topological gap so that it reaches point **d** corresponding to the edge state with negative group velocity and residing on the different edge [see Fig. 2(b) at half of the BO period].

Therefore, in the topological insulator, highly unconventional Bloch oscillations, involving switching between its opposite edges and periodic penetration into the bulk, occur. Despite the fact that the gradient is applied along the y axis only, the wave packet exhibits oscillations also along the x axis, a remarkable phenomenon that is not known to occur in nontopological systems. After point **d** is passed, the wave packet transforms into the state from the top of the first band, i.e., it expands into the bulk again [see Fig. 2(b) at three quarters of the BO period]. After reaching the $k = K$ point, the wave packet arrives to point **b** and then comes back to the initial location **c** within the topological gap (i.e., it returns to the left edge in real space), completing one BO cycle. The described dynamics clearly shows that, in complete contrast to nontopological systems or to excitations in the depth of the band of topological system, BOs involving edge states exhibit a period $T = 2K/\alpha$ that is two times larger than the period of usual BO. Thus, to return to the initial location the wave packet has to traverse the Brillouin zone twice [11].

Note that if the input state corresponds to the edge state, an inversion of the sign of the gradient does not change the direction of BOs in real space [compare Figs. 2(a) and 2(b)]. The direction of motion in the momentum space does change. Because for $\alpha < 0$ the wave packet upon evolution turns into the mode from the top of the first band (rather than into the mode from the bottom of the second band as it happened for $\alpha > 0$) one can see that the structure of the wave in the bulk on the first and second halves of BO cycles is different for opposite gradients.

In Figs. 2(c)–2(f) we plot the coordinates of the center of mass of the wave packet in real space (x_c, y_c) and in the Fourier domain (k_x, k_y) as functions of time, calculated by the

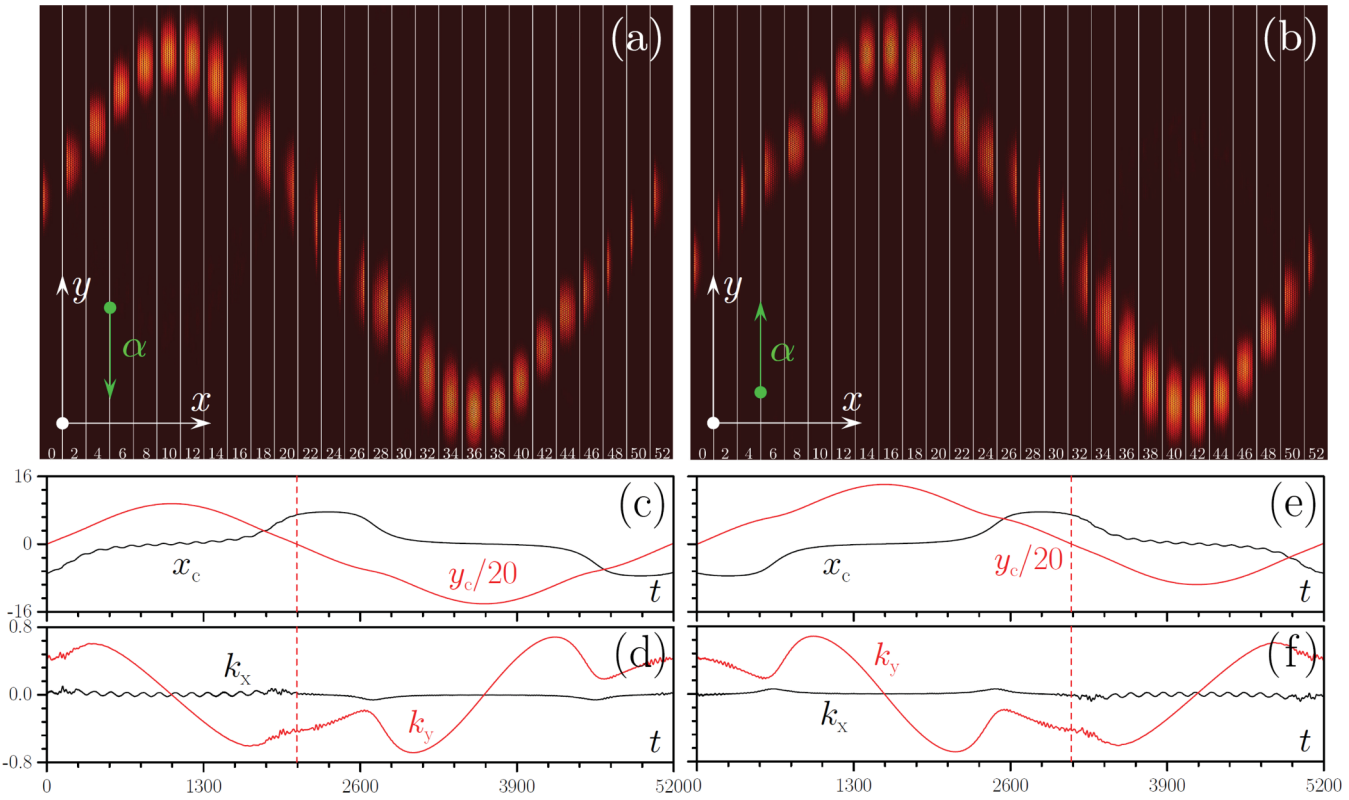

FIG. 2. Distributions of $|\psi_-|$ in different moments of time corresponding to the number of the cross section multiplied by 100 showing dynamics of Bloch oscillations for positive Zeeman splitting $\Omega = +0.8$ and gradients $\alpha = -0.001$ (a) and $\alpha = +0.001$ (b). Initially topological edge state with momentum $k = 0.4$ K and width $w = 30$ is located on the left edge. Green arrows indicate gradient direction. Red dashed lines in (c)–(f) indicate the moment of time when the wave packet returns to the $y = 0$ point, but at the opposite edge of the insulator.

expressions:

$$(x_c, y_c) = U^{-1} \iint (x, y)(|\psi_+|^2 + |\psi_-|^2)dxdy,$$

$$(k_x, k_y) = 4\pi F^{-1} \iint (\kappa_x, \kappa_y)(|\tilde{\psi}_+|^2 + |\tilde{\psi}_-|^2)d\kappa_x d\kappa_y, \quad (2)$$

where $U = \iint(|\psi_+|^2 + |\psi_-|^2)dxdy$, $F = \iint(|\tilde{\psi}_+|^2 + |\tilde{\psi}_-|^2)d\kappa_x d\kappa_y$, and $\tilde{\psi}_+, \tilde{\psi}_-$ are the Fourier transforms of ψ_+, ψ_-. The oscillations of the x coordinate of the wave packet center are out-of-phase with oscillations of its y coordinate, the amplitude of the latter being much larger [Figs. 2(c) and 2(e)]. Notice that we study a relatively narrow topological insulator to reduce the temporal period of the BO. The period can be drastically reduced by larger gradients α, but this may lead to Landau-Zener tunneling. The periodic motion of the wave packet in the spectral domain is readily visible in Figs. 2(d) and 2(f), which show a much larger variation in the k_y component. The dependencies $k_{x,y}(t)$ are perfectly periodic, indicating that the wave packet is almost exactly recovered after a BO cycle. Note that the integral criterion (2) yields smooth time dependencies of $k_{x,y}$, see Figs. 2(d) and 2(f), even when a wave packet reappears at the other edge of the Brillouin zone.

A change of sign of the Zeeman splitting, from $\Omega = +0.8$ to $\Omega = -0.8$, significantly affects the dynamics of the BOs. The spectrum $\varepsilon(k)$ remains similar to that shown in Fig. 1(e), but with several noteworthy differences. First, inverting the sign of Ω changes the relative strength of the ψ_+ and ψ_- spinor components. Second, the edge mode from the red (green) curve that resides at the left (right) edge of the array at $\Omega = 0.8$, for the opposite sign of Ω it resides on the right (left) edge. Thus, if the mode at point **c** from Fig. 1(e) is excited, one starts the BO cycle from the mode on the right edge (see Fig. 3). The y dynamics in this case remains the same, but evolution along the x axis reverses: the trajectories of motion can be obtained from those shown in Fig. 2 if one changes $x_c \to -x_c$ and $k_x \to -k_x$. Thus, the conclusion is that the magnetic field that determines the direction of edge currents can also be used to change the x component of the currents.

Figures 4(a) and 4(b) show the dependence of the complete time period T and y-amplitude A_y of BOs on the potential gradient α for a fixed spin-orbit coupling strength $\beta = 0.3$. Here T is defined as the time required for the wave packet to return to the initial position after traversing twice the Brillouin zone, while A_y is determined as a difference between the maximal and minimal y positions of the wave packet during evolution. In accordance with the model of adiabatic motion of the wave packet within the Brillouin zone caused by a constant force described above, both these parameters vary as $\sim 1/\alpha$. While the period T is independent of the spin-orbit coupling strength β, the amplitude of oscillations A_y monotonically decreases with increasing β [Fig. 4(c)]. Such a phenomenon was not expected. Indeed, the amplitude of BO is usually proportional to the maximal energy difference acquired by the wave packet upon motion across the Brillouin

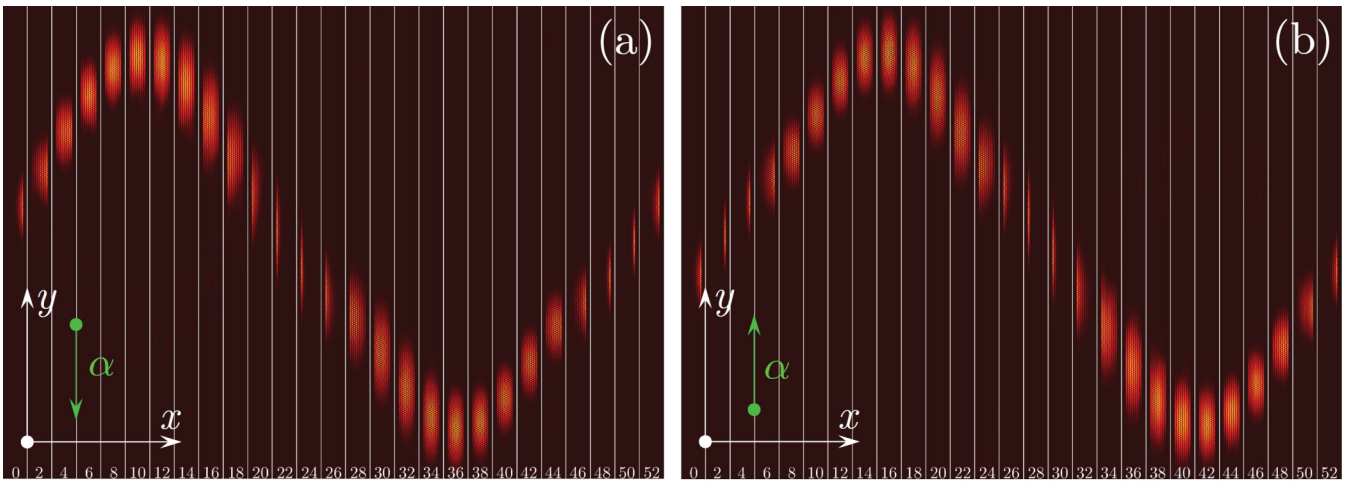

FIG. 3. Same as in Fig. 2, but for negative Zeeman splitting $\Omega = -0.8$. Initially topological edge state with momentum $k = 0.4$ K and width $w = 30$ is located on the right edge. Evolution of wave packet center and central momentum in the Fourier domain (not shown here) is identical to that shown in Figs. 2(c)–2(f), but one has to change $x_c \to -x_c$ and $k_x \to -k_x$.

zone and one may expect that the difference should grow with increasing β due to broadening of the topological gap. However, while the gap broadens with β, the two lowest bands shrink, leading to an overall decrease of the interval of energies scanned by the wave packet, which, in turn, leads to diminishing A_y.

Finally, we would like to stress that Bloch oscillations reported here can be observed even in the presence of nonlinear interactions in the low-density regime. To illustrate this we included corresponding nonlinear terms $(|\psi_\pm|^2 + \sigma|\psi_\mp|^2)\psi_\pm$ accounting for repulsion between polaritons with the same spin and weak attraction $\sigma = -0.05$ between polaritons with opposite spins into the right-hand side of the evolution Eq. (1). The dynamics of evolution within half of Bloch oscillations cycle for different input peak amplitudes $a^-_{t=0}$ of the dominating ψ_- component in this nonlinear case is shown in Fig. 5 for the same α, Ω parameters as in Fig. 2(b). Bloch oscillations clearly persist up to amplitude values $a^-_{t=0} \sim 0.1$.

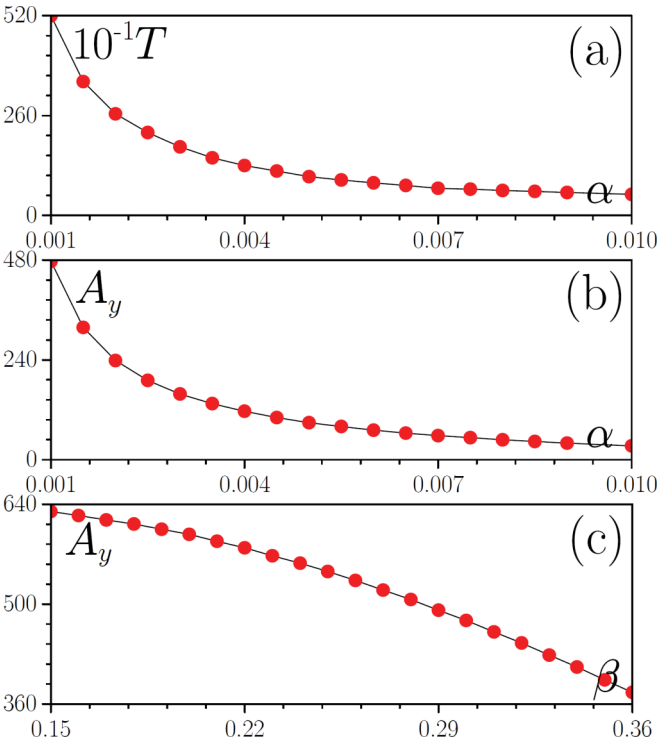

FIG. 4. Period (a) and y amplitude (b) of topological Bloch oscillations versus gradient α at $\beta = 0.3$. (c) y amplitude of Bloch oscillations versus strength of spin-orbit coupling β at $\alpha = 0.001$. In all cases $\Omega = +0.8$.

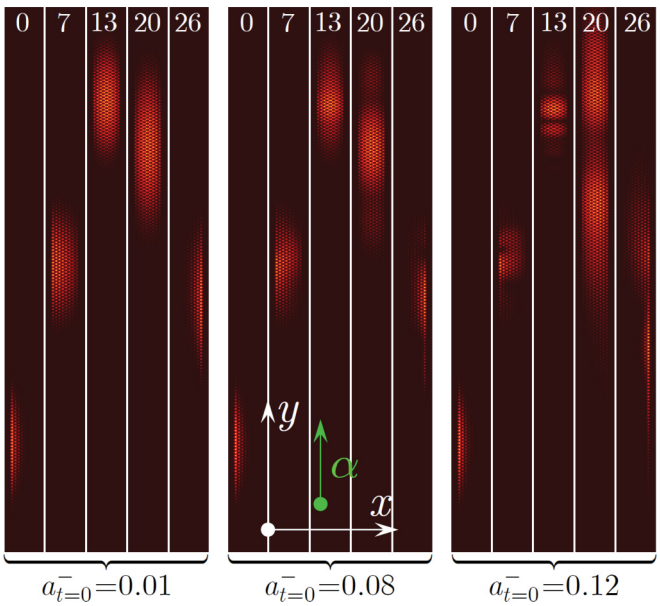

FIG. 5. Distributions of $|\psi_-|$ in different moments of time corresponding to the number of the cross section multiplied by 100 showing dynamics of *nonlinear* Bloch oscillations for $\Omega = +0.8$, $\alpha = +0.001$, and different input peak amplitudes of the ψ_- component indicated below panels. Half of the Bloch oscillations cycle is shown. Initially topological edge state with momentum $k = 0.4$ K and width $w = 30$ is located on the left edge.

For larger input amplitudes (hence stronger nonlinear effects) one observes distortions of the wave packet and its splitting into two fragments. At the same time, the wave packet still moves to the opposite edge of the ribbon after completing half of the oscillation cycle.

IV. CONCLUSION

We presented a new type of Bloch oscillations, namely Bloch oscillations of topological edge states. The fundamental result that we have uncovered is that a full cycle of Bloch oscillation for a topological edge state is achieved through a continuous transformation between the localized edge mode and the delocalized bulk mode, as well as through a transition between the two edge states. In a topological insulator the wave packet traverses the Brillouin zone twice to complete one Bloch oscillation cycle, thus the period of oscillations in a topological system is two times larger than in the usual insulator. These topology-controlled phenomena are in sharp contrast to the behavior exhibited by nontopological systems.

ACKNOWLEDGMENTS

Y.V.K. acknowledges support from the Severo Ochoa Excellence Programme (SEV-2015-0522), Fundacio Privada Cellex, Fundacio Privada Mir-Puig, and CERCA/Generalitat de Catalunya. C.L. acknowledges support of the National Natural Science Foundation of China (NSFC) (Grant No. 11805145) and Natural Science Foundation of Shaanxi Province (Grant No. 2019JQ-089). Y.V.K. acknowledges funding of this work by RFBR and DFG according to the research project No. 18-502-12080. F.Y. acknowledges support from the NSFC (Grants No. 61475101 and No. 11690033).

[1] F. Bloch, Uber die quantenmechanik der elektronen in kristallgittern, Z. Phys. **52**, 555 (1928).

[2] C. Zener, A theory of the electrical breakdown of solid dielectrics, Proc. R. Soc. London Ser. A **145**, 523 (1934).

[3] J. Feldmann, K. Leo, J. Shah, D. A. B. Miller, J. E. Cunningham, S. Schmitt-Rink, T. Meier, G. von Plessen, A. Schulze, and P. Thomas, Optical investigation of Bloch oscillations in a semiconductor superlattice, Phys. Rev. B **46**, 7252 (1992).

[4] C. Waschke, H. G. Roskos, R. Schwedler, K. Leo, H. Kurz, and K. Köhler, Coherent Submillimeter-wave Emission from Bloch Oscillations in a Semiconductor Superlattice, Phys. Rev. Lett. **70**, 3319 (1993).

[5] E. E. Mendez, F. Agulló-Rueda, and J. M. Hong, Stark Localization in GaAs-GaAlAs Superlattices Under an Electric Field, Phys. Rev. Lett. **60**, 2426 (1988).

[6] P. Voisin, J. Bleuse, C. Bouche, S. Gaillard, C. Alibert, and A. Regreny, Observation of the Wannier-Stark Quantization in a Semiconductor Superlattice, Phys. Rev. Lett. **61**, 1639 (1988).

[7] M. Ben Dahan, E. Peik, J. Reichel, Y. Castin, and C. Salomon, Bloch Oscillations of Atoms in an Optical Potential, Phys. Rev. Lett. **76**, 4508 (1996).

[8] S. R. Wilkinson, C. F. Bharucha, K. W. Madison, Q. Niu, and M. G. Raizen, Observation of Atomic Wannier-Stark Ladders in an Accelerating Optical Potential, Phys. Rev. Lett. **76**, 4512 (1996).

[9] B. P. Anderson and M. A. Kasevich, Macroscopic quantum interference from atomic tunnel arrays, Science **282**, 1686 (1998).

[10] O. Morsch, J. H. Muller, M. Cristiani, D. Ciampini, and E. Arimondo, Bloch Oscillations and Mean-field Effects of Bose- Einstein Condensates in 1D Optical Lattices, Phys. Rev. Lett. **87**, 140402 (2001).

[11] Y. V. Kartashov, V. V. Konotop, D. A. Zezyulin, and L. Torner, Bloch Oscillations in Optical and Zeeman Lattices in the Presence of Spin-Orbit Coupling, Phys. Rev. Lett. **117**, 215301 (2016).

[12] U. Peschel, T. Pertsch, and F. Lederer, Optical Bloch oscillations in waveguide arrays, Opt. Lett. **23**, 1701 (1998).

[13] R. Morandotti, U. Peschel, J. S. Aitchison, H. S. Eisenberg, and Y. Silberberg, Experimental Observation of Linear and Nonlinear Optical Bloch Oscillations, Phys. Rev. Lett. **83**, 4756 (1999).

[14] T. Pertsch, P. Dannberg, W. Elflein, A. Bräuer, and F. Lederer, Optical Bloch Oscillations in Temperature Tuned Waveguide Arrays, Phys. Rev. Lett. **83**, 4752 (1999).

[15] S. Stützer, Y. V. Kartashov, V. A. Vysloukh, V. V. Konotop, S. Nolte, L. Torner, and A. Szameit, Hybrid Bloch-Anderson localization of light, Opt. Lett. **38**, 1488 (2013).

[16] A. Joushaghani, R. Iyer, J. K. S. Poon, J. S. Aitchison, C. M. de Sterke, J. Wan, and M. M. Dignam, Quasi-Bloch Oscillations in Curved Coupled Optical Waveguides, Phys. Rev. Lett. **103**, 143903 (2009).

[17] G. Corrielli, A. Crespi, G. Della Valle, S. Longhi, and R. Osellame, Fractional Bloch oscillations in photonic lattices, Nat. Commun. **4**, 1555 (2013).

[18] H. Trompeter, W. Krolikowski, D. N. Neshev, A. S. Desyatnikov, A. A. Sukhorukov, Y. S. Kivshar, T. Pertsch, U. Peschel, and F. Lederer, Bloch Oscillations and Zener Tunneling in Two-Dimensional Photonic Lattices, Phys. Rev. Lett. **96**, 053903 (2006).

[19] Y. Sun, D. Leykam, S. Nenni, D. Song, H. Chen, Y. D. Chong, and Z. Chen, Observation of Valley Landau-Zener-Bloch Oscillations and Pseudospin Imbalance in Photonic Graphene, Phys. Rev. Lett. **121**, 033904 (2018).

[20] A. Block, C. Etrich, T. Limboeck, F. Bleckmann, E. Soergel, C. Rockstuhl, and S. Linden, Bloch oscillations in plasmonic waveguide arrays, Nat. Commun. **5**, 3843 (2014).

[21] M. Wimmer, M. A. Miri, D. Christodoulides, and U. Peschel, Observation of Bloch oscillations in complex PT-symmetric photonic lattices, Sci. Rep. **5**, 17760 (2015).

[22] M. Z. Hasan and C. L. Kane, Topological insulators, Rev. Mod. Phys. **82**, 3045 (2010).

[23] X.-L. Qi and S.-C. Zhang, Topological insulators and superconductors, Rev. Mod. Phys. **83**, 1057 (2011).
[24] L. Lu, J. D. Joannopoulos, and M. Soljačić, Topological photonics, Nat. Photon. **8**, 821 (2014).
[25] F. D. M. Haldane and S. Raghu, Possible Realization of Directional Optical Waveguides in Photonic Crystals with Broken Time- Reversal Symmetry, Phys. Rev. Lett. **100**, 013904 (2008).
[26] Z. Wang, Y. Chong, J. D. Joannopoulos, and M. Soljačić, Observation of unidirectional backscattering-immune topological electromagnetic states, Nature (London) **461**, 772 (2009).
[27] N. H. Lindner, G. Refael, and V. Galitski, Floquet topological insulator in semiconductor quantum wells, Nat. Phys. **7**, 490 (2011).
[28] M. Hafezi, E. A. Demler, M. D. Lukin, and J. M. Taylor, Robust optical delay lines with topological protection, Nat. Phys. **7**, 907 (2011).
[29] R. O. Umucalilar and I. Carusotto, Fractional Quantum Hall States of Photons in an Array of Dissipative Coupled Cavities, Phys. Rev. Lett. **108**, 206809 (2012).
[30] A. B. Khanikaev, S. H. Mousavi, W.-K. Tse, M. Kargarian, A. H. MacDonald, and G. Shvets, Photonic topological insulators, Nat. Mater. **12**, 233 (2013).
[31] M. C. Rechtsman, J. M. Zeuner, Y. Plotnik, Y. Lumer, D. Podolsky, F. Dreisow, S. Nolte, M. Segev, and A. Szameit, Photonic Floquet topological insulators, Nature (London) **496**, 196 (2013).
[32] M. A. Bandres, M. C. Rechtsman, and M. Segev, Topological Photonic Quasicrystals: Fractal Topological Spectrum and Protected Transport, Phys. Rev. X **6**, 011016 (2016).
[33] A. V. Nalitov, D. D. Solnyshkov, and G. Malpuech, Polariton Z Topological Insulator, Phys. Rev. Lett. **114**, 116401 (2015).
[34] C.-E. Bardyn, T. Karzig, G. Refael, and T. C. H. Liew, Topological polaritons and excitons in garden-variety systems, Phys. Rev. B **91**, 161413(R) (2015).
[35] T. Karzig, C.-E. Bardyn, N. H. Lindner, and G. Refael, Topological Polaritons, Phys. Rev. X **5**, 031001 (2015).
[36] O. Bleu, D. D. Solnyshkov, and G. Malpuech, Interacting quantum fluid in a polariton Chern insulator, Phys. Rev. B **93**, 085438 (2016).
[37] Y. V. Kartashov and D. V. Skryabin, Modulational instability and solitary waves in polariton topological insulators, Optica **3**, 1228 (2016).
[38] Y. V. Kartashov and D. V. Skryabin, Bistable Topological Insulator with Exciton-Polaritons, Phys. Rev. Lett. **119**, 253904 (2017).
[39] C. Li, F. Ye, X. Chen, Y. V. Kartashov, A. Ferrando, L. Torner, and D. V. Skryabin, Lieb polariton topological insulators, Phys. Rev. B **97**, 081103(R) (2018).
[40] S. Klembt, T. H. Harder, O. A. Egorov, K. Winkler, R. Ge, M. A. Bandres, M. Emmerling, L. Worschech, T. C. H. Liew, M. Segev, C. Schneider, and S. Höfling, Exciton-polariton topological insulator, Nature (London) **562**, 552 (2018).
[41] M. Atala, M. Aidelsburger, J. T. Barreiro, D. Abanin, T. Kitagawa, E. Demler, and I. Bloch, Direct measurement of the Zak phase in topological Bloch bands, Nat. Phys. **9**, 795 (2013).
[42] M. Aidelsburger, M. Lohse, C. Schweizer, M. Atala, J. T. Barreiro, S. Nascimbène, N. R. Cooper, I. Bloch, and N. Goldman, Measuring the Chern number of Hofstadter bands with ultracold bosonic atoms, Nat. Phys. **11**, 162 (2015).
[43] G. Jotzu, M. Messer, R. Desbuquois, M. Lebrat, T. Uehlinger, D. Greif, and T. Esslinger, Experimental realization of the topological Haldane model with ultracold fermions, Nature (London) **515**, 237 (2014).
[44] D. Xiao, M.- C. Chang, and Q. Niu, Berry phase effects on electronic properties, Rev. Mod. Phys. **82**, 1959 (2010).
[45] E. Arévalo and L. Morales-Molina, Bloch-Zener oscillations in ribbon-shaped optical lattices, Europhys. Lett. **96**, 60011 (2011).
[46] Y. Plotnik, M. A. Bandres, Y. Lumer, M. C. Rechtsman, and M. Segev, Topological control of Bloch oscillations of edge modes in photonic lattices, in *Conference on Lasers and Electro-Optics (CLEO)* (Optical Society of America, San Jose, 2015) paper FTu2C.4.
[47] J. Höller and A. Alexandradinata, Topological Bloch oscillations, Phys. Rev. B **98**, 024310 (2018).
[48] M. Steger, C. Gautham, D. W. Snoke, L. Pfeiffer, and K. West, Slow reflection and two-photon generation of microcavity exciton-polaritons, Optica **2**, 1 (2015).
[49] J. Kasprzak, M. Richard, S. Kundermann, A. Baas, P. Jeambrun, J. M. J. Keeling, F. M. Marchetti, M. H. Szymańska, R. André, J. L. Staehli, V. Savona, P. B. Littlewood, B. Deveaud, and L. S. Dang, Bose-Einstein condensation of exciton polaritons, Nature (London) **443**, 409 (2006).
[50] M. Wouters, I. Carusotto, and C. Ciuti, Spatial and spectral shape of inhomogeneous nonequilibrium exciton-polariton condensates, Phys. Rev. B **77**, 115340 (2008).
[51] K. G. Lagoudakis, F. Manni, B. Pietka, M. Wouters, T. C. H. Liew, V. Savona, A. V. Kavokin, R. André, and B. Deveaud-Plédran, Probing the Dynamics of Spontaneous Quantum Vortices in Polariton Superfluids, Phys. Rev. Lett. **106**, 115301 (2011).
[52] F. Baboux, D. De Bernardis, V. Goblot, V. N. Gladilin, C. Gomez, E. Galopin, L. Le Gratiet, A. Lemaître, I. Sagnes, I. Carusotto, M. Wouters, A. Amo, and J. Bloch, Unstable and stable regimes of polariton condensation, Optica **5**, 1163 (2018).
[53] B. Nelsen, G. Q. Liu, M. Steger, D. W. Snoke, R. Balili, K. West and L. Pfeiffer, Dissipationless Flow and Sharp Threshold of a Polariton Condensate with Long Lifetime, Phys. Rev. X **3**, 041015 (2013).
[54] M. Steger, G. Q. Liu, B. Nelsen, C. Gautham, D. W. Snoke, R. Balili, L. Pfeiffer, and K. West, Long-range ballistic motion and coherent flow of long-lifetime polaritons, Phys. Rev. B **88**, 235314 (2013).